High-Frequency Cyclotron Resonance in Lead and the Electron-Phonon Interaction

P. Goy and B. Castaing
*Groupe de Physique des Solides, Ecole Normale Supérieure, 24 rue Lhomond, 75231 Paris Cedex 05, France**
(Received 6 July 1972)

The frequency and temperature dependences of the electron-phonon interaction have been investigated in lead by the Azbel'–Kaner cyclotron-resonance technique. The experiments have been performed in the unusual millimeter and submillimeter microwave band from 70 to 500 GHz, corresponding to the wavelength 4 to 0.6 mm. In this frequency band the photon energy value, $\hbar\omega \leq 2$ meV, is near the typical phonon energy in lead. The experiments were performed in the temperature range from 1.5 up to 6 °K. The effective mass m^* and relaxation time τ, measured on two different types of orbits, are frequency and temperature dependent. These dependences are directly related to the electron-phonon interaction. For both orbits m^* is found to increase as the temperature squared and the frequency squared. The maximum relative increases are $m^*(5.4\,°\mathrm{K})/m^*(0\,°\mathrm{K}) = 1.03$ and $m^*(457\ \mathrm{GHz})/m^*(0\ \mathrm{GHz}) = 1.008$. The relaxation frequency τ^{-1} dependence varies as the cube of both the temperature and the frequency. The theoretical dependences on T and ω are thus well confirmed, but the order of magnitude of the frequency effects is smaller than predicted.

I. INTRODUCTION

In metals at low temperature, the observed cyclotron mass m^* is generally larger than expected following the band model. This discrepancy is mainly attributed to the electron-phonon interaction.[1]

The electron-phonon-interaction strength depends upon the distance of the quasiparticle from the Fermi level, and various authors have predicted the frequency[2] and the temperature[3] dependence of the cyclotron effective mass m^*, and of the electronic relaxation time τ. These effects are supposed to be observable when the distance of the quasiparticle from the Fermi level $\hbar\omega$ or k_BT is comparable to the Debye energy (k_B is the Boltzmann constant). The amplitude of the expected effects is enhanced in the case of a metal with a strong electron-phonon interaction, such as lead.

The essential information concerning both the electron-phonon interaction and the phonon spectrum is contained in the function $\alpha^2(\omega)F(\omega)$. $\alpha(\omega)$ represents the energy-dependent electron-phonon coupling constant, and $F(\omega)$ the phonon density of states for phonons of frequency ω. The quantity $\alpha^2(\omega)F(\omega)$ has been experimentally determined for lead by the tunneling technique.[4] Its shape [Fig. 1(a)] is not very different from that of the phonon spectrum $F(\omega)$. Both have a peak in energy due to transverse phonons near $E_t \approx 4.4$ meV; this energy corresponds to 51 °K and to the microwave frequency 1000 GHz, or the wavelength 0.3 mm.

The changes of the electron-phonon interaction strength are expected to be observable on m^* and τ when $\hbar\omega$ or k_BT is comparable to E_t. Observation of the frequency effects clearly requires very high frequencies, which until recently were not available. Besides, such high frequencies are needed in the temperature experiment to observe well-defined cyclotron resonances, with the short relaxation time at finite temperature.

The purpose of this paper is to present the results of an Azbel' –Kaner[5] cyclotron-resonance experiment, which measured the frequency and temperature dependences of the cyclotron effective mass m^* and of the electronic relaxation time τ in lead. These experiments, which provide new experimental evidence for the mass enhancement due to the electron-phonon interaction, were performed at frequencies from 70 to 460 GHz, and at temperatures between 1.5 and 6 °K. The upper frequency and temperature values correspond to $\hbar\omega = 0.43E_t$ and $k_BT = 0.12E_t$, respectively.

The arrangement of this paper is as follows. In Sec. II is presented a brief theory of the electron-phonon interaction in metals. In Sec. III is described the experimental arrangement, including an original millimeter and submillimeter spectrometer. In Sec. IV the experimental results in lead are presented. In Sec. V a theory for the direct comparison between temperature and frequency effects is given, followed by a summary and the conclusion in Sec. VI.

II. BRIEF THEORY OF ELECTRON-PHONON INTERACTION IN METALS

A. Electron-Phonon Interaction at the Fermi Level $\lambda(\omega = 0, T = 0)$

First, let us look at the electron-phonon interaction at the Fermi level, i.e., $T = 0$ and $\omega = 0$, where $\hbar\omega$ is the energy distance from the Fermi level. The observed cyclotron mass m^* is generally larger than the band-calculated mass m_b. For instance, in sodium with a spherical Fermi surface, the experimental value[6] is $m^* = 1.24m_0$, instead of m_0 the free-electron mass. This dis-

crepancy is mainly attributed to the electron-phonon interaction,[1] the electron-electron interaction being weak in metals. In the following the usual notations are employed.[1-4]

The electron-phonon interaction strength can be measured by means of the renormalization coefficient λ defined as follows: The observed mass m^* is

$$m^* = (1+\lambda)m_b \quad . \tag{1}$$

The maximum value $\lambda \approx 1.5$ is found in the two strong-coupling superconductors mercury and lead.[7]

The presence of electron-phonon interaction modifies the dispersion relation of the free carriers. The eigenvalues of the Hamiltonian do not correspond purely to electrons but, because of the interaction, to mixed electron-phonon states. For this quasiparticle, the electron is called dressed or surrounded by a cloud of virtual phonons.

In terms of the band structure let us call the single-particle energy $\epsilon_{\vec{k}}$, where $\vec{k}$ is the wave vector. Taking into account the interaction, the new energy $E_{\vec{k}}$ is the single-particle energy $\epsilon_{\vec{k}}$ plus a complex term Σ_{e-ph} called self-energy:

$$E_{\vec{k}} = \epsilon_{\vec{k}} + \Sigma_{e-ph}(\vec{k}, E_{\vec{k}}) = \epsilon_{\vec{k}} + M_{e-ph}(\vec{k}, E_{\vec{k}}) - i\,\Gamma_{e-ph}(\vec{k}, E_{\vec{k}}). \tag{2}$$

Assuming that the $\vec{k}$ dependence of the real part M of Σ is negligible, we can obtain λ at the Fermi level by

$$\lambda(T=0,\ \omega=0) = -\left.\frac{\partial M_{e-ph}(\omega)}{\partial \omega}\right|_{E_F} \quad . \tag{3}$$

The imaginary part Γ of the complex self-energy Σ gives the quasiparticle lifetime, i.e., the phonon-limited relaxation time

$$\tau_{e-ph} = \hbar/2\Gamma_{e-ph}(\omega) \quad . \tag{4}$$

The real M and the imaginary Γ parts of the self-energy Σ are related by Kramers–Kronig relations. Their variations[3] versus ω depend upon the shape of the phonon density spectrum $\alpha^2(\omega)F(\omega)$. In lead, at zero temperature $-M_{e-ph}(\omega)$ starts linearly from the origin with the slope $\lambda(T=0,\ \omega=0)=1.5$ given by the well-known formula[7]

$$\lambda(T=0,\ \omega=0) = 2\int_0^\infty [\alpha^2 F(\omega)/\omega]\, d\omega \quad . \tag{5}$$

Then $-M_{e-ph}(\omega)$ increases, goes through a maximum at $\omega = E_t$ due to the transverse phonon peak, and decreases after a second maximum at $\omega = E_l$ due to the longitudinal phonon peak [Fig. 1(b), solid line]. The energy of longitudinal phonons is approximately $E_l \approx 2E_t$. $\Gamma(\omega)$ is small for the small energies ω, increases abruptly between $\frac{1}{2}E_t$ and $2E_t$, and is constant with its maximum value for the high energies. At finite temperature[3] the variations are

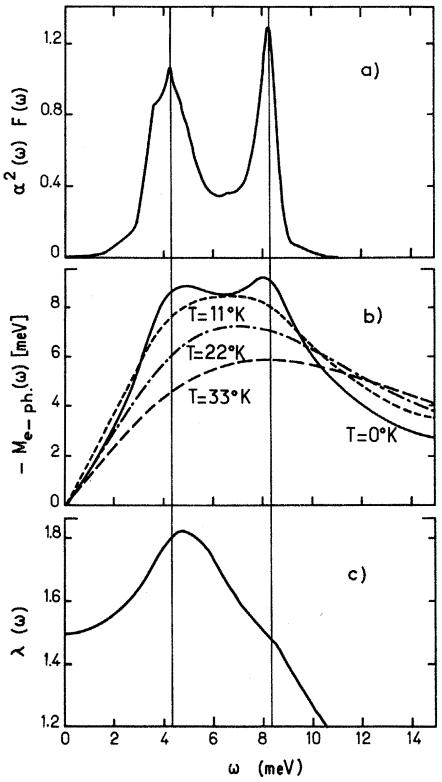

FIG. 1. (a) Effective electron-phonon interaction $\alpha^2(\omega)F(\omega)$ for lead deduced from superconducting tunneling experiment by McMillan and Rowell (Ref. 4). (b) The real part of the self-energy $-M_{e-ph}(\omega, T)$ for lead at different temperatures calculated by Grimvall (Ref. 3). (c) The renormalization coefficient $\lambda(\omega)$ versus frequency for lead, calculated by Allen at zero temperature (Ref. 10).

smoother [Fig. 1(b), dashed lines] and $\Gamma(\omega)$ has a finite value even for the small energies ω.

The electron-phonon interaction distorts the band structure $E_{\vec{k}}$, relative to the single-particle band structure $\epsilon_{\vec{k}}$, in a very small region of typical energy $\hbar\omega \approx 2E_t$ about the Fermi energy. The cyclotron-resonance mass is proportional to the derivative of the Fermi-surface section A versus energy, taken at the Fermi energy E_F:

$$m^* = \frac{\hbar^2}{2\pi}\left.\frac{\partial A}{\partial \epsilon}\right|_{E_F} \quad . \tag{6}$$

Therefore this technique samples the distorted region and gives a mass which deviates from the single-particle mass m_b. Experimental results,[8] as compared to the band-model predictions,[9] qualitatively confirm the large value of λ in lead.

Such deviation is expected to be both temperature and frequency dependent since, as ω increases, a wider range of the distorted region is sampled, while as T increases the distortion of $E_{\vec{k}}$ changes.

B. Electron-Phonon Interaction above the Fermi Level $\lambda(\omega, T)$

In other words, the electronic self-energy $\Sigma_{e\text{-}ph}$ is a function of the energy distance ω from the Fermi level, and of the temperature T. This is clearly seen on Fig. 1(b). Therefore the electron-phonon strength can vary. Rather than measuring the electron-phonon interaction at the Fermi level and zero temperature, we are only interested in this experiment in the changes of the electron-phonon interaction strength. These changes are observed when the temperature T, or the frequency ω, used in our experiment gives an equivalent energy $k_B T$ or $\hbar\omega$ comparable to the typical phonon energy $E_t \approx 4.4$ meV in lead.

1. *Frequency Effects* $\lambda(\omega)$.

In the presence of the microwave radiation ω we can say, roughly speaking, that the quasiparticle energy is increased by $\hbar\omega$. Therefore the quasiparticle energy above the Fermi level can be tested by varying the microwave frequency ω. The theory has been developed by Scher and Holstein in the case of a metal with spherical Fermi surface and Debye phonon spectrum.[2]

In a recent paper,[10] Allen has calculated the $\lambda(\omega)$ and $\tau_{e\text{-}ph}(\omega)$ variations in lead from the experimental $\alpha^2(\omega)F(\omega)$ function.[4] Starting from its value of 1.5 the renormalization coefficient $\lambda(\omega)$ increases with a parabolic shape in the ω range $0\text{-}\frac{1}{2}E_t$, has a maximum of 1.8 for the energy value E_t which corresponds to the first phonon peak, and decreases towards zero for high ω values [Fig. 1(c)].

Clearly, one would like to observe the increase of λ with frequency and subsequent decrease towards zero for the highest ω. But, because of the increase of the imaginary part of the self-energy, the particle lifetime $\tau_{e\text{-}ph}$ decreases rapidly when increasing ω. In our technique we need a large $\omega\tau$ value, so the cyclotron-resonance experiment is possible only for the lower ω values, i.e., the increasing part of $\lambda(\omega)$. Our microwave band is in the good region, since for our highest frequency $\hbar\omega = 0.43E_t$, a large value $\omega\tau_{e\text{-}ph} \approx 80$ is still predicted in lead.[10]

2. *Temperature Effects* $\lambda(T)$

The electronic distribution is broadened by $k_B T$ around the Fermi level; therefore, the number of available states for transition is increased. That is the physical reason why the predicted effects for a finite temperature T are stronger than for the equivalent frequency ω with $k_B T = \hbar\omega$.

Using the experimental[4] $\alpha^2(\omega)F(\omega)$ function in lead, Grimvall[3] has calculated the temperature dependence of the normalization coefficient. The variations of $\lambda(T)$ can be deduced from the slope at the origin of $-M_{e\text{-}ph}(\omega)$ on Fig. 1(b), according to Eq. (3). The renormalization coefficient $\lambda(T)$ also first increases and then decreases towards zero, with the same pattern as $\lambda(\omega)$ given in Fig. 1(c); but the maximum is reached at a temperature T_M with $k_B T_M \approx \frac{1}{4}E_t$. Since E_t corresponds to 51 °K, we have $T_M \approx 13$ °K, and for this temperature the maximum value $\lambda(T_M) = 1.7$ is predicted.

At the same time, the predicted relaxation-time decay due to finite temperature T is faster than the decay due to finite frequency ω.

Let us summarize this brief comment on theory: The enhancement factor λ can vary with frequency and temperature. With increasing ω or T, $\lambda(\omega, T)$ first increases, reaches a maximum, and then decreases down to zero. In the cyclotron-resonance technique, because of the correlated relaxation-time decay, the only observable shifts will correspond to increasing λ.

The predicted maximum relative shifts $\Delta\lambda/\lambda$ are nearly the same in many metals.[11] The observable quantity is the effective mass m^*. According to Eq. (1), the relative change in m^* will be given by

$$\Delta m^*/m^* = [\lambda/(1+\lambda)]\Delta\lambda/\lambda \quad . \tag{7}$$

Any shift in λ can be seen in m^* but λ has to be large to give an easily observable shift in m^* because of the factor $\lambda(\lambda+1)$. From this point of view, the best metals are mercury and lead[7] with $\lambda \approx 1.5$.

Several significant experiments versus T have been performed in the metals Zn,[12] Pb,[13,14] and Hg,[15] not including semimetals.

In a previous paper,[16] we have reported the first frequency experiment performed in mercury and lead in the frequency range 30–300 GHz. We could not see, in lead, any change in the effective mass because of our poor accuracy ($\mp 0.7\%$). Besides, the relaxation-time dependence $\tau^{-1}_{e\text{-}ph} \propto \omega^2$ observed in lead was not correct. In fact, for the very large $\omega\tau$ obtained at low temperature with our highest frequencies, the narrow resonance widths can unfortunately be broadened easily because of the nonperfect sample flatness, magnetic field inhomogeneity, modulation amplitude, etc. Therefore the obtained relaxation time, proportional to the experimental linewidth, was lowered too much with frequency.

In this paper we present the first experiment which has been performed as a function of T and ω together. By working with these two adjustable parameters, we can check most of the experimental results and improve the final accuracy, especially that of the relaxation time. In addition, the T and ω dependences observed in a single sample on a single orbit, with identical experimental conditions, can be directly compared with the theoretical predictions (see Sec. V).

III. EXPERIMENTAL ASPECTS

A. Sources

To perform our experiments[17,18] in the wavelength band from 2 to 0.6 mm, we use carcinotrons from Thomson-C.S.F. Co. They are backward-wave oscillators and give the highest frequencies produced by vacuum electronic tubes. In the electromagnetic wave spectrum, carcinotrons are located between klystrons and lasers.

The four carcinotrons we have used give the approximate wavelengths 2, 1, 0.8, and 0.6 mm with the maximum microwave power 4, 1, 0.01, and 0.06 W, respectively. Table I gives the frequencies used, with their equivalent values expressed in different units.

The emission band of a carcinotron $\omega_2 \geq \omega \geq \omega_1$ has a typical broadness $(\omega_2 - \omega_1)/\omega \approx 0.1$. The microwave frequency ω increases versus beam voltage with the approximate rate $\delta\omega/\omega\delta V \approx 3\times10^{-5}$ V^{-1}. Unfortunately, the microwave power P, available at the output of those carcinotrons, is strongly dependent on beam voltage V, with very sharp peaks. Therefore, a well-stabilized high-voltage power supply[19] is used: $V = 2-12$ kV ∓ 0.1 V.

The typical relative microwave stability is of the order of $\Delta P/P \lesssim 10^{-4}$ when the voltage V is adjusted exactly on one peak of the $P(V)$ characteristics. The relative frequency stability is

$$\Delta\omega/\omega = \Delta V \delta\omega/\omega\,\delta V = 3\times10^{-6} \quad \text{with } \Delta V = 0.1 \text{ V}. \tag{8}$$

Because of the peaked-power spectrum of the carcinotron, it is difficult to devise a good locking feedback mechanism. Therefore, our general arrangement (Fig. 2) is very simple, especially if we compare it with the usual lower-frequency spectrometers.

B. General Arrangement

A 4-mm waveguide is used between the source and the experimental cavity. The sample (Sec. III F) is fixed between the poles of a magnet and is cooled to liquid-helium temperatures; its plane surface and a copper spherical mirror fixed in front of it define a Fabry–Perot cavity (Sec. III C). A carbon bolometer glued on the sample gives a signal directly related to the real part R of the surface

TABLE I. Frequencies of the different microwave sources used in this experiment and their equivalent corresponding values in different units.

F (GHz)	ω (10^{12} sec^{-1})	λ (mm)	ν (cm^{-1})	E (meV)	T (°K)
73	0.46	4.1	2.4	0.3	3.5
136	0.85	2.2	4.5	0.56	6.5
270	1.7	1.1	9	1.1	13
386	2.4	0.77	13	1.6	18.5
456	2.9	0.65	15	1.9	22

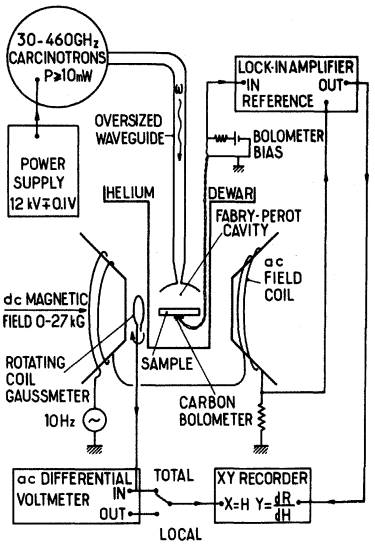

FIG. 2. General schematic diagram of the experimental setup.

impedance (Sec. III E). The field-modulation technique is quite classical. The synchronously detected signal dR/dH is recorded versus the magnetic field H.

The magnet, a Harvey–Wells model No. L158, can be rotated around the Dewar. H is measured by the ac voltage induced in a rotating coil probe. The relative accuracy, based upon the precise voltage measure given by an ac differential voltmeter (Precision Standard Corp. model No. CSC 1002), is better than $\mp 0.01\%$. The magnetic field at resonance is taken on an average of about 10 recordings, and its final relative accuracy is $\mp 0.015\%$ in the best cases.

The resonance linewidths, which give the relaxation time τ, are difficult to measure precisely since they are very sensitive to the signal-to-noise ratio; our accuracy is about $\pm 7\%$.

C. Cavity

For the wavelengths between 2 and 0.6 mm, our 4-mm waveguide is oversized. At the lower end of the waveguide (Fig. 3), a small-angle cone reduces the dimension of the oversized waveguide to the size ϕ_c of a single-mode waveguide. (ϕ_c is of the order of the wavelength.) This cone terminates on a coupling iris of diameter ϕ_t and thickness e, pierced through the spherical reflector of the cavity. ($\phi_t \approx \frac{1}{3}\lambda$ and $e \approx \frac{1}{10}\phi_t$.) The spherical reflector is made out of copper and polished on an optical surface of suitable radius of curvature R. Its transverse diameter ϕ_M is less than 20 mm in order to fit in the Dewar.

Because of our wavelength band, we have chosen the optical-type Fabry–Perot cavity. Moreover,

this type of cavity allows us to work in a wide-frequency range. We can continuously cover the interval between 30 and 500 GHz.

Let us remark that a high quality factor Q is undesirable in our experiments, because of the absence of any locking of the emitted frequency to the cavity frequency. The frequency fluctuations of the source give power fluctuations inside the cavity

$$\Delta P'/P = Q^2(\Delta\omega/\omega)^2 \quad . \tag{9}$$

Q is voluntarily reduced to several thousand by a reduction of the reflectors's distance d below the semiconfocal geometry, and by overcoupling the cavity with an enlarged coupling iris. Typically, $d \approx 3$ mm and $Q \approx 3000$. The noise due to frequency fluctuations is then $\Delta P'/P \approx 10^{-4}$, following Eqs. (8) and (9), and is of the same order of magnitude as the noise due to power fluctuations.

Table II summarizes the typical dimensions used in our Fabry–Perot cavity (Fig. 3). For a given wavelength λ, the sample diameter ϕ_S has to be smaller than a maximum in order to avoid secondary modes, and larger than a minimum in order to make the cavity resonance possible. Practically, we choose $\phi_S = 19$ mm in the wavelength range 9–1 mm, and $\phi_S = 10$ mm in the wavelength range 4–0.6 mm.

D. Mountings

The parallelism between the magnetic field and the sample surface is, in some cases, very critical in observing the Azbel'–Kaner cyclotron resonance. For this reason, the vertical sample geometry is usual with the magnet rotating around a vertical axis [Fig. 4(a)]. In our experiment, the most difficult observable quantity is the frequency dependence of the effective mass $m^*(\omega)$. When changing the frequency, it is necessary to change the cone and the spherical reflector of the cavity. This is not possible without removing the sample in the geometry of Fig. 4(a). In successive experiments one could observe some change in the effective mass because of a slightly different crystalline orientation of the sample along the magnetic field.

In the second mounting, especially designed to observe the small variations of $m^*(\omega)$, the sample is horizontal [Fig. 4(b)]. Screwing or unscrewing

TABLE II. Dimensions of the Fabry-Perot cavity given in mm. The symbols are referred to in the text and shown in Fig. 2. λ is the microwave wavelength.

λ	ϕ_c	ϕ_t	e	ϕ_M and ϕ_S optimum	ϕ_S minimum	ϕ_S maximum
9	8	2.2	0.3	19	19	>20
4.1	4	1.2	0.2	19	9	>20
2.2	2	0.7	0.1	14	5	19
1.1	0.8	0.35	0.05	9	4	19
0.77–0.66	0.6	0.25	0.03	6	3	12

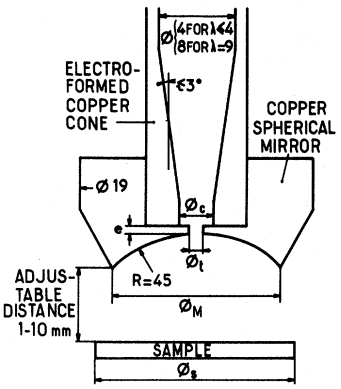

FIG. 3. Detail of the Fabry–Perot cavity. The symbols are referred to in the text. The different dimensions are listed in Table II and given in mm.

the control tube changes the position of the spherical reflector, and permits the tuning of the cavity. Also, the conical transition and the spherical mirror can be removed and changed, in order to work with another microwave frequency, while the sample remains cooled and fixed in the cryostat.

The angle between the horizontal surface and the horizontal magnetic field is less than 0.5° but can-

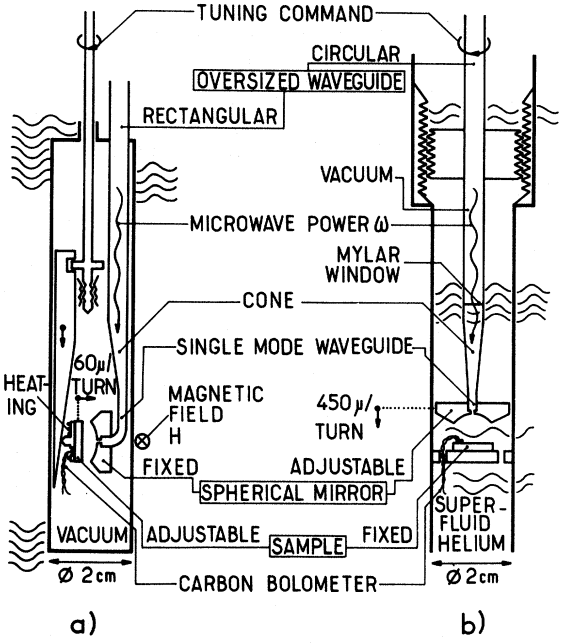

FIG. 4. Two types of mounting used: (a) The sample is mounted in a vacuum enclosure to allow experiments at different temperatures. (b) The entire system is immersed in superfluid helium. The spherical mirror and the conical transition can be easily removed and changed, while the sample remains fixed and cooled in the cryostat. This mounting is especially convenient to obtain the frequency dependence of the effective mass.

not be corrected. We have verified, with the first mounting, that this point is of no importance in the case of the studied orbits in lead, traced on cylindrical parts of the Fermi surface. The line shape and the linewidth are not changed by tipping angles as large as $\mp 0.7°$.

In the second mounting, the Fabry–Perot cavity is immersed in liquid helium. To avoid any bubble inside the cavity, the temperature is kept below the superfluid transition point.

In the first mounting [Fig. 4(a)], the sample is mounted in a vacuum enclosure in order to allow experiments at different temperatures. The thermal contact between the sample and the cooling helium bath is maintained by a low-pressure helium exchange gas.

The sample is heated either by the adjustable microwave power, or by a heater resistor which is glued on its brass support. For a given temperature, the observed effects are exactly the same with microwave heating and resistor heating.

E. Detector and Sensitivity

Since the detector is in the magnetic field, the carbon-type bolometer has been chosen because of its low magnetoresistance ($\Delta r/r \approx 0.05$ at 30 kG). The small 0.1-W 100-Ω Allen–Bradley resistor is used. It is first reduced to the parallelepipedic shape $3\times1\times0.25$ mm. Its value $r(T)$ is then around 1 kΩ at room temperature. The bolometer, insulated by a 9-μm Mylar sheet, is glued on the sample using GE 7031 varnish.

For $r(300\ °K) \approx 1$ kΩ we obtain $r(4.2\ °K) \approx 20$ kΩ and $r(1.5\ °K) \approx 600$ kΩ. Around a fixed temperature T,

$$dr/r = -\alpha\, dT/T \ , \tag{10}$$

where

$$\alpha \simeq 3.9 \quad \text{for } 1.5\ °K \leq T < 2.8\ °K \tag{10a}$$

$$\simeq 2.4 \quad \text{for } 2.8\ °K \leq T < 5\ °K \ . \tag{10b}$$

The sample temperature T is given by

$$T = T_0 + T_1 \ , \tag{11}$$

where T_0 is the bath temperature and T_1 the increase in temperature due to the absorbed microwave power P:

$$T_1 = P/KS \ . \tag{12}$$

K is the thermal resistance per surface unit between the bath and the sample and S is the sample area. Since $dP/P = dR/R$, where R is the real part of the surface impedance, Eqs. (10)–(12) give

$$\frac{dr}{r} = -\frac{\alpha\, dR/R}{1 + T_0/T_1} \ . \tag{13}$$

The maximum observed relative change at resonance is $\Delta R/R \approx 10^{-2}$. This small value confirms that our thermally detected signal is quite linear versus the surface impedance, following Eq. (13).

For a typical microwave power 250 mW at the output of the source, the power absorbed in the sample is 5 mW, due to the losses in the transmission and in the copper mirror, making a rise in temperature [Eq. (12), $T_1 = 0.1\ °K$] when the sample is placed in superfluid helium. When the sample is placed in the vacuum enclosure, T_1 is about 10 times greater.

If the heating due to the microwave is 0.1 °K above 1.5 °K, the change in bolometer voltage, due to the maximum surface impedance change $\Delta R/R = 10^{-2}$ at resonance, is $\Delta V = 2.5$ mV [with 1-V typical bolometer voltage, and according to Eqs. (10a) and (13)]. With a modulation amplitude of about a $\frac{1}{25}$ of the resonance linewidth, the largest ac detected signal has an amplitude $\frac{1}{25}(2.5\ \text{mV}) = 100$ μV. This last value is the order of magnitude of the sensitivity range used on the lock-in amplifier. The heat capacity of the sample is not taken into account in the ac response calculated here, since the thermal relaxation time C/KS around 10^{-3} sec is very short as compared to the modulation period 0.1 sec.

Using a lock-in amplifier, the sensitivity is usually $\Delta R/R = 10^{-5}$; in the best conditions with our better source at 270 GHz, $\Delta R/R = 10^{-6}$ which gives a synchronously detected change $\Delta T \approx 10^{-7}$ K.

F. Samples

Lead single crystals have been grown in a quartz and stainless-steel mold.[20] They have disc shapes 1 mm thick, and 17- and 10-mm diameters for the samples used in this experiment, numbers 13 and 20, respectively.

The quality of the surface grown against an optically polished quartz plate depends on the carbon layer deposed on the quartz plate in order to avoid any sticking between the cooled metal and the quartz. Too much carbon makes the surface dirty.

The lead purity is 99.9999% (Cominco), and the residual resistivity ratio is deduced from our results (Sec. IV E) as $4–7\times10^4$.

IV. RESULTS

A. Orbits Studied

The Fermi surface of lead consists of a closed-hole surface in the second zone and a multiply connected electron-tubes surface in the third zone.[9] Many different masses can be visible in the cyclotron-resonance experiment.[8]

The crystallographic orientation has been chosen so that only two masses appear, to avoid overlapping in subharmonic series at high frequency or high temperature. For both samples the magnetic field is placed along [110] axis. The largest

signals are due to a ζ orbit[8] traced on the smallest section of an electron tube in the third zone of the Fermi surface, with the minimum cyclotron mass observable in lead $m^* \approx 0.56 m_0$. The smallest resonance signals are due to a ψ type[8] orbit on the closed-hole sheet in the second zone, with $m^* \approx 1.2 m_0$ (Fig. 5). For sample 20 the surface orientation has been chosen in order to make the ψ orbit resonance more effective for ψ orbit studies (Fig. 6).

B. Line Shape

Because of the small number of resonant electrons owing to the complicated shape of the lead Fermi surface, one observes Chambers's resonance line shape[21] as soon as $\omega_c \tau$ is large enough, where ω_c is the cyclotron frequency and τ the relaxation time. According to Chambers, $\omega_c \tau \geq 50$ is a necessary condition to observe this line shape.

For magnetic field variations very close to the resonance, this condition can be less severe (Fig. 7).[22] In lead for ζ and ψ orbits, we experimentally verified on the successive subharmonics n, where $\omega_c \tau$ decreases as n^{-1}, that the effective mass m^* and the relaxation time τ can be precisely measured following the theoretical Chambers's line shape for $\omega_c \tau \geq 12$.

Both ζ and ψ orbits obey the same line shape (Chambers's mass "minimum",[22] $\alpha < 0$), but the agreement between experimental and theoretical line shapes (Fig. 7) is better for the ζ orbit than for the ψ orbit. Following the theoretical line shape, if ΔH is the linewidth and A the amplitude from the minimum to the maximum in dR/dH, the exact resonance magnetic field is $0.355 \Delta H$ less than the maximum in dR/dH, and is located at $0.306A$ under the maximum. The product $\omega\tau$ is measured by the Chambers's formula

$$\omega\tau = 1.55 H_n / \Delta H \ . \tag{14}$$

C. Magnetic Field Conditions

For Azbel'-Kaner cyclotron-resonance studies, the magnetic field range is limited by a maximum and a minimum, since the resonance is possible only if the time of flight of the resonant electrons in their passage through the skin layer is small compared with the rf period. This condition can break down at low field, where the orbit curvature is small (retardation effects[23-25]), and at very high field, where the orbit is totally inside the skin layer (local conditions).

In our case the smaller orbit is ζ. Its average diameter in real space equals the skin depth $\delta \approx 0.05$ μm for the magnetic field 600 kG. Thus the nonlocal conditions are well fulfilled in our experiments for both orbits at any magnetic field between 0 and 27 kG.

It is shown in the following that retardation effects,[23-25] clearly visible below 4 kG for the upper

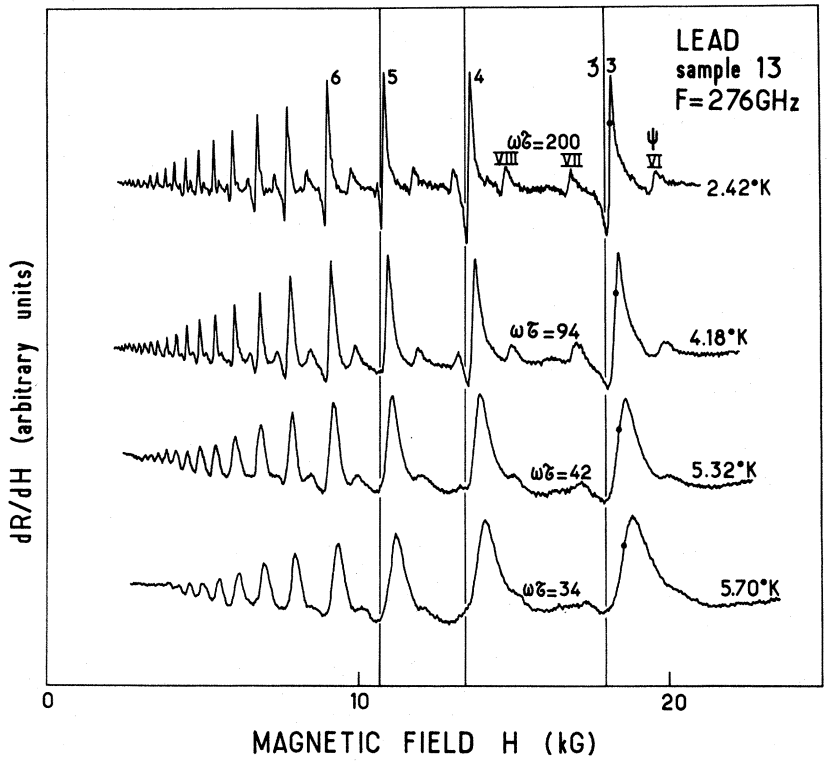

FIG. 5. Cyclotron-resonance traces obtained at 276 GHz for various temperatures. The vertical lines are the extrapolated positions of the subharmonics at zero temperature. The black spots indicate the precise resonance-field position. When the temperature increases, this position is shifted towards higher field, showing the correlated mass increase. The resonance width increases with temperature because of the correlated relaxation-time decay.

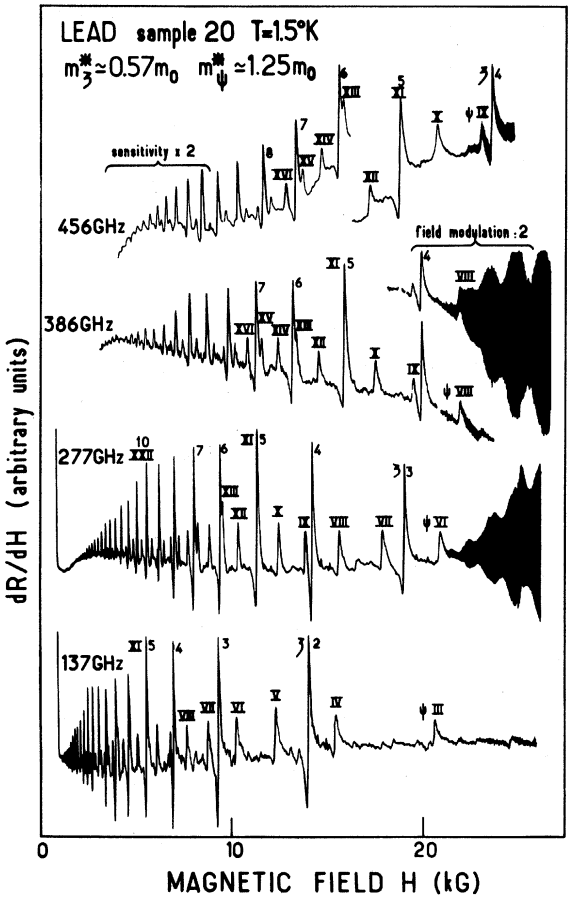

FIG. 6. Cyclotron-resonance traces obtained at various frequencies. The large peaks series are due to the ζ orbit. Arabic numbers give their subharmonic order. The small peak series are due to the ψ orbit. Their subharmonic order is labeled with Roman numbers. Above 20 kG, quantum oscillations are visible (Appendix B). The field modulation amplitude is slightly reduced above 15 kG, so the amplitude decay of the cyclotron resonance is not significant in the high-field region.

frequencies, cannot change significantly the experimental results measured in the magnetic field range around 20 kG.

Because of retardation effects, the resonance disappears when the transit time t of the electrons in their passage through the skin layer δ becomes longer than the microwave period $T = 2\pi/\omega$, which is especially short at high frequency. The transit length in the skin layer is $2(2R_c\delta)^{1/2}$

$$t = 2(2R_c\delta)^{1/2}/V_F \ . \qquad (15)$$

Let us define a typical retardation magnetic field H_R making $t = T$. For our nearly circular orbits, R_c is related to the effective mass and to the magnetic field as in the free-electron case, and we obtain

$$H_R = 2c\omega^2\delta m^*/\pi^2 eV_F \ . \qquad (16)$$

In lead, with an effective mass $m^* \approx 0.56m_0$, a Fermi velocity $V_F \approx 5\times10^{-5}$ m/sec, and a skin depth $\delta \approx 5\times10^{-8}$ m, Eq. (16) gives $H_R \approx 1.8$ kG at 277 GHz. The resonances are effectively observed down to 2 kG at this frequency (Fig. 8).[26]

In the anomalous skin effect conditions, δ varies as $\omega^{-1/3}$, so H_R given by Eq. (16) varies as $\omega^{5/3}$. The observed magnetic field cutoff obeys this $\omega^{5/3}$ law at high frequency (Fig. 8, arrows).

Retardation effects do not affect only the resonance amplitude but they change the line shape. For our highest frequency 456 GHz, the cyclotron-resonance signal disappears near the 21st subharmonic with $t \approx T$ (Fig. 8), so $t \approx 0.4T$ for the fourth subharmonic Eq. (15). The corresponding retardation angle ϕ defined in Ref. 25 is 34°. The amplitude decay versus subharmonic number[25] gives approximately the same ϕ. For a greater retardation $\phi = 45°$, the Chambers's line shape[21] should be changed from a $\alpha < 0$ type to a $\alpha = 0$ type.[25] In our experiment, no change is observed for the considered fourth subharmonic at 456 GHz [Fig. 9(a)].

But, for the lower-field subharmonics, ϕ increases, and we attribute to retardation effects the less deep minimum in dR/dH for high-order subharmonics (such as for the $\alpha = 0$ type), especially at the upper frequencies (Figs. 6 and 8).

In any case, for the frequency experiment where retardation can occur, the resonance sharpness makes the line-shape problem less crucial: If a $\alpha = 0$ Chambers's line shape[21] is analyzed as if

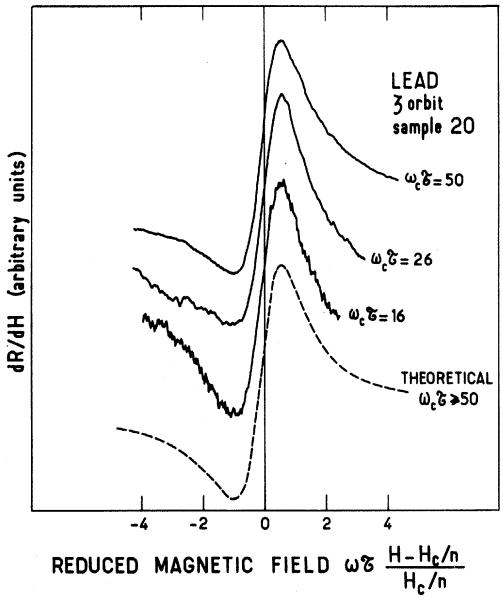

FIG. 7. Comparison between theoretical and experimental line shape. The experimental traces have been obtained on the second subharmonic of ζ orbit at 73 GHz for various temperatures.

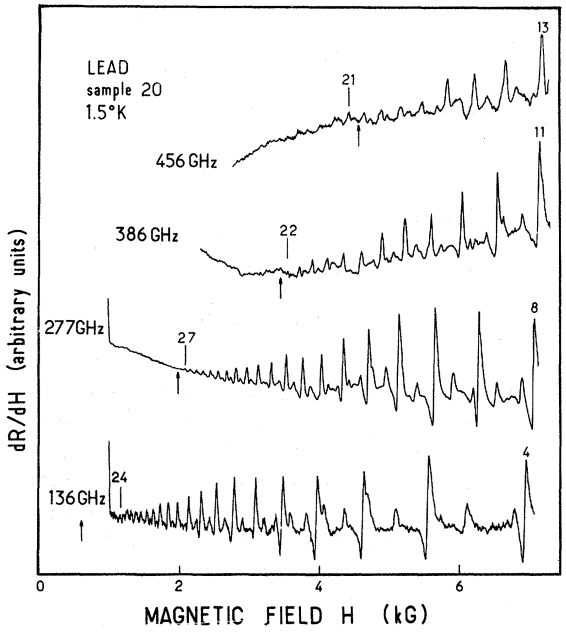

FIG. 8. Cyclotron-resonance traces obtained with various frequencies in the low magnetic field region showing retardation effects. Above each trace, the numbers give the subharmonic order for the dominant ζ orbit. The position of the last visible subharmonic is marked by a vertical line. Below each trace the arrow corresponds to the predicted $H \propto \omega^{5/3}$ law.

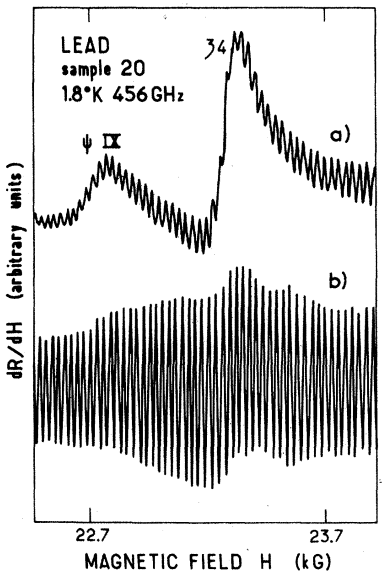

FIG. 9. Quantum oscillations and cyclotron resonance due to the same ζ orbit. (a) The modulation amplitude, larger than the short dHvA period, reduces the size of the quantum signal relative to the cyclotron-resonance signal. (b) The modulation is decreased by a factor of 5. The vertical sensitivity is the same as in (a). In this last case, the resulting relative size of the signals is unchanged with a still lowered modulation.

$\alpha < 0$, the relative error in field position is $-0.2/\omega\tau$, making the measured mass 0.07% too small for our $\omega\tau = 290$ at 456 GHz, and the relaxation time 6% too large.

Practically, we can conclude that the retardation effects can slightly decrease the experimental accuracy in the frequency experiment, but cannot significantly change the experimental results. Proofs of this point are that there is practically no change in the resonance line shape at high field for the upper frequency [Fig. 9(a) compared to Fig. 7], and that, for a given frequency, the measurements performed on different subharmonics following the same line shape give the same m^* and τ results.

D. Effective-Mass Results

1. *Temperature Experiments*

Figure 5 shows the experimental traces obtained for a fixed frequency 276 GHz at different temperatures. In Fig. 10 are shown the details of another experiment at 136 GHz with the second and third subharmonics. In Fig. 10, we can verify Chambers's theoretical prediction,[21] that there is no magnetic field dependence of the amplitude, the line shape, the relative linewidths, or shifts.

The temperature has been measured by the lead superconducting transition observed in surface impedance. The critical magnetic field between 803 and 0 G is a nearly[27] parabolic function of the temperature in the range 0–7.2 °K. The temperature accuracy (Figs. 11 and 12) is better towards higher temperature $\Delta T = \mp 0.05$ °K at 5.5 °K, and $\Delta T = \mp 0.15$ °K at 1.6 °K. During each run the tem-

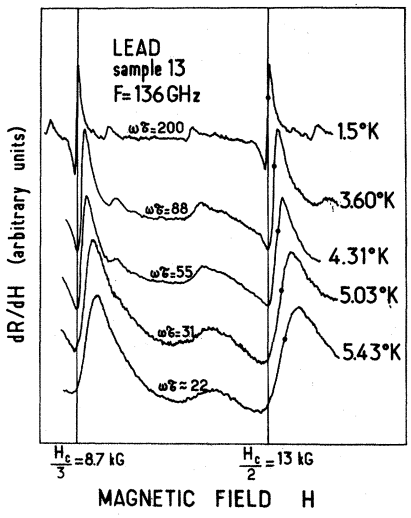

FIG. 10. Detail of the second and third subharmonics traces at 136 GHz for various temperatures. The vertical lines are the low-temperature positions.

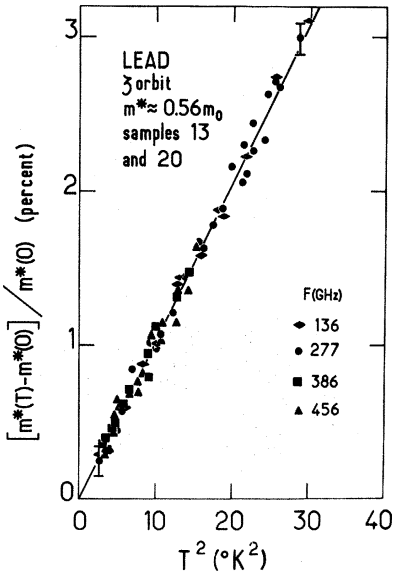

FIG. 11. Effective-mass enhancement as a function of T^2 obtained at various frequencies on the ζ orbit.

perature stability has been found to be better than 0.05 °K.

The temperature experiments have been performed at four different frequencies on the same ζ orbit in two different samples (Fig. 11). The relative mass increase with T is parabolic, and is exactly the same for any frequency. This point is a good check of the exact position of the resonance magnetic field on the resonance line, since different ω give different $\omega\tau$ at the same temperature, and would give different mass shifts with an incorrect plot.

The mass variations for ζ orbit are

$$m^*(T) = m^*(0)\,(1 + q\,T^{2\mp 0.1}) \ , \tag{17}$$

$$q = (1.03 \mp 0.05)\,10^{-3}\ {}^\circ\mathrm{K}^{-2} \ . \tag{17a}$$

The $m^*(T)$ dependence investigated on the ψ orbit obeys the same law [Eqs. (17) and (17a)] with a slightly lowered accuracy (Fig. 12).

2. *Frequency Experiments*

In Fig. 6, we report several experimental traces obtained at the same low temperature with different microwave frequencies. For a given subharmonic, for instance, the fourth of ζ orbit, we can see that the field position is nearly proportional to the frequency, and the frequency dependence of the cyclotron mass is not visible. The effective-mass variations will appear in slight changes of the resonance field multiplied by the microwave wavelength. This wavelength is measured after the cyclotron-resonance experiment by means of an original semiconfocal Fabry–Perot transmission wavemeter. Any wavelength between 4 and 0.6 mm can be measured within the relative accuracy $\mp 0.015\%$. The resonance field is measured with the same accuracy $\mp 0.015\%$. This accuracy is better than in the temperature experiment, since the large $\omega\tau$ around 300 obtained at low temperature gives sharp peaks.

Therefore the small total experimental uncertainty obtained on the relative $m^*(\omega)$ measure performed in the second mounting [Fig. 4(b)] is

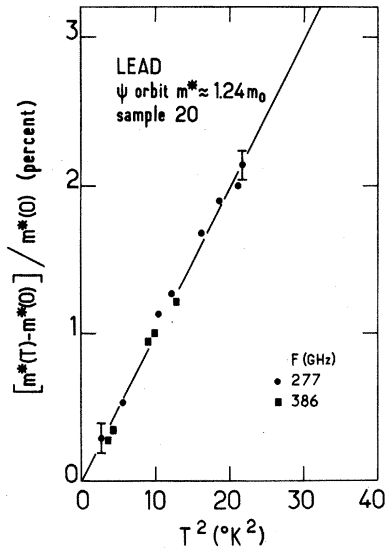

FIG. 12. Effective-mass enhancement as a function of T^2 obtained at two different frequencies on the ψ orbit. The solid line has the same slope as in Fig. 11.

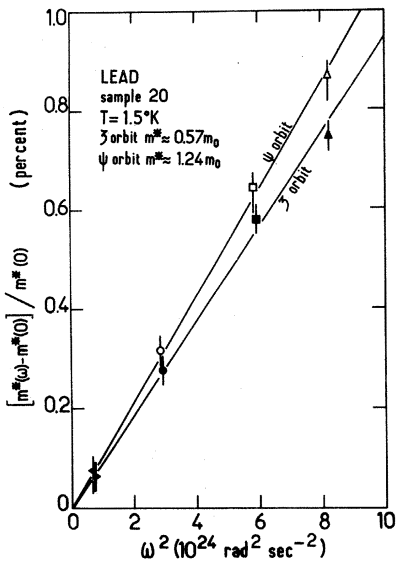

FIG. 13. Effective-mass enhancement as a function of ω^2 obtained on the ζ and ψ orbits.

$\mp 0.03\%$. It permits us to observe a parabolic increase of the effective mass with the microwave frequency ω (Fig. 13). There is a slight anisotropy visible between the ψ and the ζ orbits. For the ζ orbit we have

$$m^*(\omega) = m^*(0)\,(1 + p\,\omega^{2^{+0.1}_{-0.3}})\ , \tag{18}$$

$$p = (9.4 \mp 0.4)\,10^{-28}\ \mathrm{sec^2/rad^2}\ . \tag{18a}$$

According to Eqs. (17)–(18a), the following formula summarizes the temperature and frequency dependences of the effective mass for the ζ orbit in the temperature and frequency ranges 0–5.5 °K and 0–460 GHz:

$$m^*(T,\omega)/m^*(0,0) = 1 + 2.7\ E_t^{-2} \times[(k_B T)^2 + (\tfrac{1}{8}\hbar\omega)^2]\ , \tag{19}$$

where the energy E_t characterizes the typical phonon energy in lead

$$E_t/k_B = 51\ ^\circ\mathrm{K}\ . \tag{20}$$

The uncertainties in Eq. (19) can be deduced from Eqs. (17)–(18a).

Note that the frequency effects are small compared to the temperature effects. For instance, the maximum relative-mass increase is about 0.8% for the highest frequency. This value is very small compared to the value 3% reached at 5.4 °K, especially if we remember that the temperature that corresponds to our highest frequency is 22 °K (Table I).

E. Relaxation-Time Results

The relaxation time τ has been measured following Eq. (14) in the temperature experiments performed successively at different microwave frequencies. The observed relaxation frequency τ^{-1} varies as the number of phonons. We have plotted the τ^{-1} values versus T^3 (Fig. 14).

The ω^3 diagram (Fig. 15) is obtained by taking τ^{-1} versus ω positions at different temperatures in the first T^3 diagram. The τ^{-1} value for $T=0$ and $\omega=0$ is the impurity relaxation frequency τ_0^{-1}. It has to be subtracted to obtain the pure electron-phonon relaxation frequency $\tau_{e\text{-}ph}^{-1}$ following the classical formula

$$\tau_{e\text{-}ph}^{-1} = \tau^{-1} - \tau_0^{-1}\ , \tag{21}$$

with

$$\tau_0 = (4 \mp 0.4)\times 10^{-10}\ \mathrm{sec},\ \text{sample 20} \tag{22}$$

$$= (7 \mp 1)\times 10^{-10}\ \mathrm{sec},\ \text{sample 13}\ . \tag{23}$$

These impurity-limited relaxation times can be related to the conductivity[28] and give the residual resistivity ratio.

For $T < 4.2$ °K, the temperature variations of the relaxation frequency, obtained at low-microwave frequency, obey the law

$$\tau_{e\text{-}ph}^{-1}(T) = a\,T^{3\mp 0.3}\ , \tag{24}$$

with the following values for the ζ orbit:

$$a = (1.32 \mp 0.1)\times 10^8\ ^\circ\mathrm{K}^{-3}\,\mathrm{sec}^{-1},\ \text{sample 20} \tag{24a}$$

$$= (1.72 \mp 0.2)\times 10^8\ ^\circ\mathrm{K}^{-3}\,\mathrm{sec}^{-1},\ \text{sample 13}\ . \tag{24b}$$

For the ψ orbit with sample 20 we obtain

$$a = (1.76 \mp 0.2)\times 10^8\ ^\circ\mathrm{K}^{-3}\,\mathrm{sec}^{-1}\ . \tag{24c}$$

The frequency variations of the relaxation frequency at zero temperature obey the law

$$\tau_{e\text{-}ph}^{-1}(\omega) = b\,\omega^{3\mp 0.3}\ . \tag{25}$$

By extrapolation to zero temperature we obtain

$$b = (2.2 \mp 0.2)\times 10^{-28}\ \mathrm{sec}^2\ \text{for } \zeta \text{ orbit}\ , \tag{25a}$$

$$= (3.6 \mp 0.8)\times 10^{-28}\ \mathrm{sec}^2\ \text{for } \psi \text{ orbit}\ . \tag{25b}$$

As previously observed on the mass dependences, the temperature and frequency laws are the same, but frequency effects are small compared to temperature effects.

The T and ω mass dependences previously described are quite independent [Eq. (19)]. Conversely, there appears for τ a crossed term: The slope of τ^{-1} versus T^3 increases with the microwave frequency (Fig. 14), and consequently the slope of τ^{-1} versus ω^3 increases with the temperature T (Fig. 15). The solid lines in Figs. 14 and 15 correspond to the following formula, approximately valid for the ζ orbit in the temperature and frequency ranges

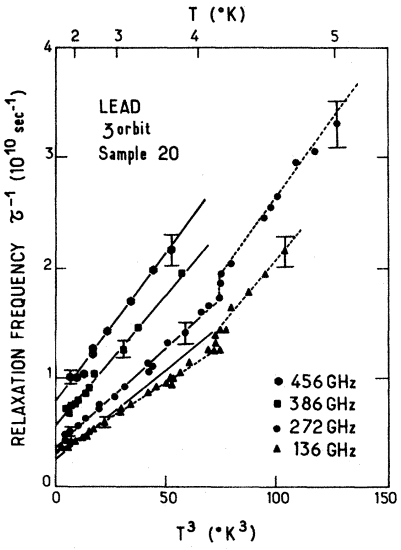

FIG. 14. Relaxation-frequency variations as a function of T^3 for different frequencies. The solid lines correspond to Eq. (26).

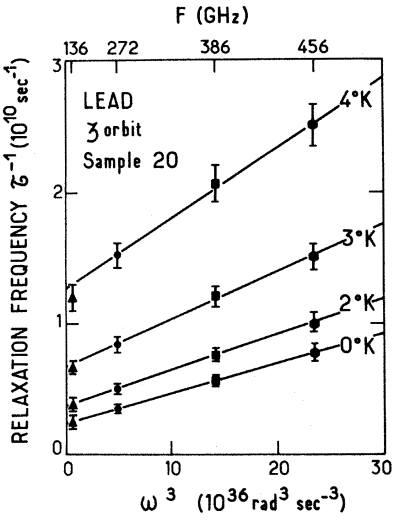

FIG. 15. Relaxation-frequency variations as a function of ω^3 for different temperatures. The solid lines correspond to Eq. (26).

0–4.2 °K and 0–460 GHz:

$$\hbar\,\tau_{e\text{-}ph}^{-1}(T,\omega)=3.25\,E_f^{-2}\left[(k_BT)^3+(\tfrac{1}{7}\hbar\omega)^3+(\hbar\omega)^3(T/25\,^\circ\mathrm{K})^3\right]\ . \qquad (26)$$

The uncertainties in Eq. (26) can be deduced from Eqs. (24) and (25).

For the ψ orbit, according to Eqs. (24c) and (25b), $\tau_{e\text{-}ph}^{-1}$ increases a little faster, but the relative contributions of the temperature and of the frequency correspond to Eq. (26).

Above the temperature (4.25 ∓ 0.1) °K, Eqs. (24)–(26) are no longer valid. The experimental points in Fig. 14 obtained at 136 and 270 GHz make new lines with increased slopes. This phenomenon has been observed on the ζ orbit with both samples. The signal-to-noise ratio for ψ orbit is too poor at this temperature to know if this phenomenon is orbit dependent. We cannot explain such an abrupt change in the $\tau(T)$ law. A phenomenon such as umklapp diffusion should give a progressive deviation to the T^3 law.

In a previous paper[29] we had reported that this change in slope of τ^{-1}/T^3 near 4.2 °K was not observed at low frequency, 73 GHz. This result was due to the lack in resolution of the resonance lines with high temperature and low frequency at 73 GHz above 4.2 °K.

F. Comparison between Observed and Predicted Effects

The effective mass and lifetime are both temperature dependent and frequency dependent. In a theoretical paper[30] magnetic field dependences are predicted. No field dependence appears experimentally.

In Fig. 16 the observed variations of the electron-phonon interaction are summarized with solid lines for ζ orbit. (For ψ orbit the variations are practically the same.)

The upper part of the figure corresponds to the renormalization coefficient λ relative to its value of 1.5 at the Fermi level and zero temperature. The lower part represents the relaxation-time variations: γ is the observed phonon-limited relaxation $\tau_{e\text{-}ph}$ [Eqs. (24) and (24b)] versus temperature at zero frequency, δ is the observed $\tau_{e\text{-}ph}$ [Eqs. (25) and (25a)] versus frequency at zero temperature. The dashed lines are the theoretically predicted dependences. Grimvall's predictions[3] (Fig. 16 lines *b* and *d*) are made especially for the temperature dependence of cyclotron resonance, while Allen's calculation[10] (Fig. 16 lines *b* and *d*) for frequency effects are intended to explain a far-infrared absorption experiment in lead.[31]

The horizontal axis is the distance from the

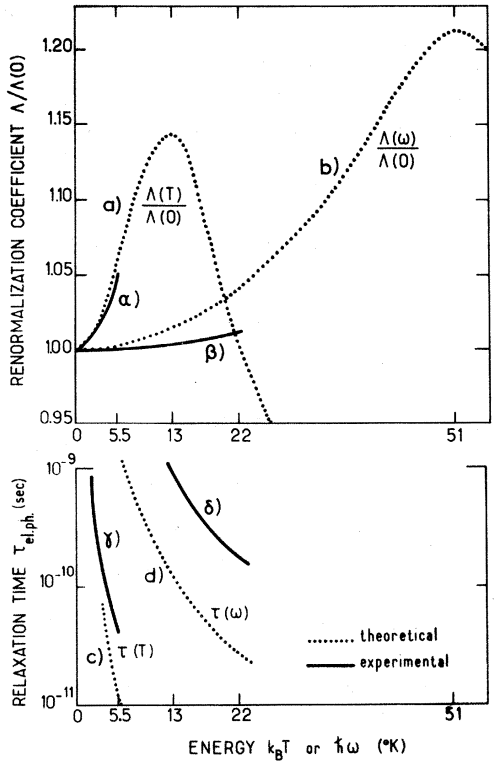

FIG. 16. Temperature and frequency dependences of the renormalization coefficient and of the relaxation time. Comparison between predicted and observed effects. The solid lines are the experimental results (see Sec. IV) for the ζ orbit, respectively at zero frequency and zero temperature. α and β are given in Eq. (19); γ and δ are given in Eq. (26). The dashed lines are the predicted variations: *a* and *c* are the temperature dependences following Grimvall (Ref. 3); *b* and *d* are the frequency dependences following Allen (Ref. 10).

Fermi level $\hbar\omega$ or $k_B T$ expressed in °K. E_t is the well-known first phonon peak energy in lead given by Eq. (20).

The observed mass change with temperature is in good agreement with the theoretical prediction (Fig. 16, α and a).

The observed mass change with frequency is small compared to the predicted one (Fig. 16, β and b). Note that in the case of the frequency effect the theoretical calculation is much more complicated than for temperature effect.

The relaxation-time decays are both slower than predicted by a factor of about 4 for the T experiment (Fig. 16, γ and c) and 7 for the ω experiment (Fig. 16, δ and d). Concerning this discrepancy, we have to consider that the theoretical calculations of τ for low T or ω are based upon the low-energy part of the $\alpha^2 F$ function, which is not precisely determined by tunneling technique. In any case, we can explain about one-half of this discrepancy by a slight error in Grimvall's and Allen's predictions. In their calculations[3,10] the classical conductivity Azbel'-Kaner[5] resonant term

$$\sigma \propto \coth\pi(i\omega/\omega_c + 1/\omega_c\tau) \tag{27}$$

is replaced by an average over states concerned:

$$\sigma' \propto \int d\epsilon \frac{f(\epsilon) - f(\epsilon+\hbar\omega)}{\hbar\omega} \coth\pi\left(i\frac{\hbar\omega + M(\epsilon) - M(\epsilon+\hbar\omega)}{\hbar\omega_c} + \frac{\Gamma(\epsilon)+\Gamma(\epsilon+\hbar\omega)}{\hbar\omega_c}\right), \tag{28}$$

where M and Γ are the real and imaginary parts of the self-energy $\Sigma_{e\text{-}ph}$ defined in Eq. (2). For small ω the oscillatory term inside coth in Eq. (28) can be written $i(1+\lambda)\,\omega/\omega_c$ according to Eq. (3); with the same conditions the damping term can be written $1/\omega_c\tau_{e\text{-}ph}$ according to Eq. (4). Therefore, in Eq. (28), the enhancement factor $1+\lambda$ appears in the oscillatory term and not in the damping term. For this reason, the predicted[3,10] relaxation time is about 2.5 times smaller than the observable phonon-limited relaxation time $\tau_{e\text{-}ph}$ defined in Eq. (21). Therefore the discrepancy between predicted relaxation-time decays[3,10] and observed variations can be reduced. The c and d branches (Fig. 16) are to be translated towards γ and δ respectively, by about one-half of the distance from them to γ and δ branches.

V. THEORETICAL DIRECT COMPARISON BETWEEN TEMPERATURE AND FREQUENCY EFFECTS

A. General Considerations

The previous theoretical work predicts the changes in the cyclotron effective mass or in the relaxation time, either for temperature variations[3,11] or for frequency variations.[2,10] In this section a simple calculation is presented which predicts both temperature and frequency effects together, and which can be used directly to analyze our observed effects. In this section ω is the microwave frequency and ω' is the integration variable.

The first-order formula for the self-energy is[3]

$$\Sigma(\epsilon) = \hbar \int d\epsilon' \int d\omega'\, \alpha^2 F(\omega') \left(\frac{1 - f(\epsilon') + N}{\epsilon - \epsilon' - \hbar\omega' + i\delta} + \frac{f(\epsilon') + N}{\epsilon - \epsilon' + \hbar\omega' + i\delta} \right). \tag{29}$$

f is the Fermi distribution and N the Bose distribution. Let us use the classical approximation

$$f(\epsilon) = \theta(-\epsilon) - \tfrac{1}{6}\pi^2 (k_B T)^2 \delta'(\epsilon), \tag{30}$$

where θ is the Heaviside function and δ' the derivative of the Dirac distribution. According to Eq. (1), a comparison between Eqs. (27) and (28) leads to the approximation

$$\lambda(T,\omega) = \int d\epsilon \frac{f(\epsilon) - f(\epsilon+\hbar\omega)}{\hbar\omega} \frac{M(\epsilon) - M(\epsilon+\hbar\omega)}{\hbar\omega}, \tag{31}$$

$$\frac{\hbar}{\tau(T,\omega)} = \frac{1}{1+\lambda(T,\omega)} \times \int d\epsilon \frac{f(\epsilon) - f(\epsilon+\hbar\omega)}{\hbar\omega} [\Gamma(\epsilon) + \Gamma(\epsilon+\hbar\omega)]. \tag{32}$$

B. Effective-Mass Dependence

According to Eqs. (29)–(31), we obtain

$$\lambda(T,\omega) = A(\omega) + \tfrac{1}{6}\pi^2 (k_B T)^2 B(\omega), \tag{33}$$

$$A(\omega) = 2\int d\omega' \frac{\alpha^2 F(\omega')}{\omega'} \left(\frac{\omega'^2}{\omega^2} \ln\left| 1 - \frac{\omega^2}{\omega'^2} \right| + \frac{\omega'}{\omega} \ln\left| \frac{\omega'+\omega}{\omega'-\omega} \right| \right), \tag{34}$$

$$B(\omega) = \frac{8}{\hbar^2} \int d\omega' \frac{\alpha^2 F(\omega')}{\omega'} \frac{1}{\omega'^2 - \omega^2}. \tag{35}$$

Developing in powers of ω, we find

$$A(\omega) = 2\int d\omega' \frac{\alpha^2 F(\omega')}{\omega'} + \frac{\omega^2}{3} \int d\omega' \frac{\alpha^2 F(\omega')}{\omega'^3}. \tag{36}$$

Since $\hbar\omega$ is small compared to the first phonon peak energy,

$$B(\omega) \approx \frac{8}{\hbar^2} \int d\omega' \, \frac{\alpha^2 F(\omega')}{\omega'^3} \quad . \tag{37}$$

For $T=0$ and $\omega=0$, Eqs. (33) and (36) give $\lambda(0,0) = A(0)$ corresponding to Eq. (5).

At low energy, following the Debye model $\alpha^2 F(\omega) \propto \omega^2$, the term $\int d\omega' \, \alpha^2 F(\omega')/\omega'^3$ is not defined. In our temperature range, the low-energy (<1 meV) part of $\alpha^2 F(\omega)$ gives a negligible contribution to the mass enhancement. Equations (5), (33), (36), and (37) give

$$\lambda(T,\omega) = \lambda(0.0) + \left(\frac{4\pi^2}{3} \int d\omega' \, \frac{\alpha^2 F(\omega')}{\omega'^3}\right) \times \left[(k_B T)^2 + \left(\frac{\hbar\omega}{2\pi}\right)^2\right] \quad . \tag{38}$$

Our experimental result (19) is in good agreement with Eq. (38): The dependences of m^* are parabolic in T and ω; the variations are independent of each other. The order of magnitude of observed effects is in good agreement with theoretical calculation, but the relative contribution of the frequency dependence is smaller than our prediction: $(\frac{1}{8}\hbar\omega)^2$ instead of $(\hbar\omega/2\pi)^2$, relative to $(k_B T)^2$.

In the very low-temperature range (0.7–2.6 °K) Krasnopolin and Khaikin[13] have determined a mass increase very close to our result, but following a $T^{1.7\mp0.2}$ law. In this temperature range, the contribution of the low-energy part of $\alpha^2 F(\omega)$ is no longer negligible. According to calculations with a parabolic $\alpha^2 F(\omega)$ dependence, the mass increases as $T^2 \ln(T_0/T)$. Similarly, the frequency dependence given by Eq. (34) is $\omega^2 \ln(\omega_0/\omega)$.

The $T^{1.7}$ law can be explained, since the logarithmic term gives a curvature of the m^*/T^2 ratio. In our frequency and temperature ranges, the curvatures cannot appear, since the logarithmic terms are practically constant.

C. Relaxation-Time Dependence

Following Eqs. (29)–(32), we obtain

$$\hbar/\tau(T,\omega) = \frac{2\pi\hbar}{1+\lambda(T,\omega)} \int d\epsilon \, \frac{f(\epsilon) - f(\epsilon+\hbar\omega)}{\hbar\omega} \int d\omega' \, \alpha^2 F(\omega') [2N + 1 + f(\epsilon+\hbar\omega') - f(\epsilon-\hbar\omega')] \quad . \tag{39}$$

In Eq. (39) the $\lambda(T,\omega)$ variations can be neglected. Moreover, in our case $\hbar\omega > kT$, so we can write

$$\begin{aligned} \frac{\hbar}{\tau(T,\omega)} &= \frac{2\pi\hbar}{1+\lambda(0,0)} \int d\omega' \, \frac{\alpha^2 F(\omega')}{\hbar\omega} \int d\epsilon \, [f(\epsilon) f(\epsilon+\hbar\omega)] [f(\epsilon - \hbar\omega') + f(\hbar\omega' - \epsilon)] \\ &\quad + \frac{4\pi\hbar}{1+\lambda(0,0)} \int d\omega' \, \frac{\alpha^2 F(\omega')}{\exp(\hbar\omega'/k_B T) - 1} \\ &\simeq \frac{2\pi\hbar}{1+\lambda(0,0)} \int_0^{\omega} d\omega' \, \frac{\omega - \omega'}{\omega} \, \alpha^2 F(\omega') + \frac{4\pi\hbar}{1+\lambda(0,0)} \int d\omega' \, \frac{\alpha^2 F(\omega)}{\exp(\hbar\omega'/k_B T) - 1} \\ &\quad + \frac{\pi\hbar}{1+\lambda(0,0)} \int \frac{d\omega'}{\hbar\omega} \, \frac{(\omega' - \omega)\, \alpha^2 F(\omega')}{\sinh[\hbar(\omega' - \omega)/2k_B T]} \exp - \left|\frac{\hbar(\omega' - \omega)}{2k_B T}\right| \quad . \end{aligned} \tag{40}$$

At high energy ω', in the integrals of Eq. (40), $\alpha^2 F(\omega')$ is multiplied by a factor $\propto \exp(-\hbar\omega'/k_B T)$, which decreases much more rapidly with ω' than the factor $(1/\omega')^3$ [Eqs. (36) and (37)]. For this reason, the τ dependence is mainly due to the parabolic low-energy part of $\alpha^2 F(\omega)$, which is negligible for the mass dependence in our case in lead. In the low-energy range, according to the Debye model

$$\alpha^2 F(\omega) = a(\hbar\omega)^2 \quad . \tag{41}$$

Equations (40) and (41) give the theoretical dependences

$$\frac{\hbar}{\tau(T,\omega)} = \frac{9.6\pi a}{1+\lambda(0,0)} \left[(k_B T)^3 + (\hbar\omega/3.9)^3 + 0.343\, \hbar\omega (k_B T)^2\right]. \tag{42}$$

Our experimental result (26) is in approximately good agreement with Eq. (42). The relative contribution of the frequency dependence is far smaller than our prediction: $(\hbar\omega/7)^3$ instead of $(\hbar\omega/3.9)^3$, relative to $(k_B T)^3$. Moreover, the experimental crossed term $T^3\omega^3$ [Eq. (26)] does not correspond to the predicted one $T^2\omega$ [Eq. (42)].

VI. SUMMARY AND CONCLUSION

The electron-phonon interaction strength depends upon the distance of the quasiparticle from the Fermi level. For this reason, the effective mass and the electronic relaxation time evidently depend upon the microwave frequency ω used for the cyclotron-resonance experiment. They depend also upon the temperature T since a finite temperature broadens the Fermi level.

When ω or T increases, the predicted effective mass first increases, and then decreases. The maximum in mass is reached when the frequency equals the typical phonon frequency (1060 GHz in lead), or the temperature equals one-fourth (13 °K in lead) of the equivalent temperature. (The typical phonon energy is the energy of the transverse phonon peak in the phonon density spectrum, $E_t = 4.4$ meV in lead.)

The relaxation-time dependence is a rapidly decreasing function of ω and T. Therefore the only observable mass variation by the cyclotron-resonance technique corresponds to the increasing part of the effective-mass dependences.

The order of magnitude of the phonon energy in metals imposes the use of very high-microwave frequencies, even in the case of the low-Debye temperature of lead. Moreover, with a high frequency ω it is possible to observe well-defined cyclotron resonance with large $\omega\tau$, even with a low relaxation time τ, because of collisions with phonons at finite temperature.

With our unusual high-frequency spectrum, the frequency experiment and the high-temperature experiment were possible. The experimental variations of the temperature and frequency effects have been measured together in lead.

The dependences of the cyclotron effective mass $m^*(T, \omega)$ and of the electric relaxation time $\tau(T, \omega)$ on two different types of orbits have been determined in the temperature and microwave-frequency range 1.5–5.5 °K and 73–456 GHz.

For both orbits the experimental mass variations are

$$m^*(T, \omega)/m^*(0,0) = 1 + 2.7\ E_t^{-2}[(k_B T)^2 + (\hbar\omega/8)^2] \ .$$

The T^2 and ω^2 terms for this mass law are easily understood. The theoretically determined frequency coefficient should be slightly greater $(\hbar\omega/2\pi)^2$.

For one orbit, the experimental relaxation-frequency variations are

$$\hbar\tau_{e\text{-}ph}^{-1}(T, \omega) = 3.2\ E_t^{-2}[(k_B T)^3 + (\tfrac{1}{7}\hbar\omega)^3 + (\hbar\omega)^3 (T/25\ ^\circ\mathrm{K})^3] \ .$$

The T^3 and ω^3 terms for the relaxation-frequency law are clearly predicted, but theory and experiment do not agree with the frequency coefficient [theoretical value $(\hbar\omega/3.9)^3$] and with the crossed term (theoretical ωT^2 instead of experimental $\omega^3 T^3$).

ACKNOWLEDGMENTS

The authors wish to thank G. Weisbuch for having provided the samples and A. Libchaber for many helpful discussions and reviewing the manuscript. Thanks are also due to H. Thomé for technical assistance and J. Brochard for machining the most delicate parts of the apparatus. We particularly thank Dr. T. Yeou, Dr. A. Shaer, and Dr. G. Guérin from Thomson-C. S. F. Co. for their assistance.

APPENDIX A: VERY RECENT EXPERIMENTAL RESULTS

In order to check our experimental accuracy, we have done an experiment at various frequencies in copper, a metal with low electron-phonon coupling and high Debye temperature. We have chosen the crystalline direction H parallel to the [111] axis, where the belly orbit giving the same Chambers's line shape "mass minimum"[32] can be observed.

In the band 136–456 GHz at 1.5 °K, the measured effective mass is constant within the experimental accuracy $\mp 0.03\%$. From the lower to the upper frequency the measured relaxation frequency τ^{-1} shows a small increase (+20%), which is not very far from the total experimental uncertainty ($\mp$ 14%) and is quite negligible compared to the value reached in the same case in lead (+150%).

This experiment in copper permits us to conclude that the misleading effects, such as the frequency dependences of the relaxation time due to surface defects, or of the effective mass due to retardation effects, are quite negligible compared to the large electron-phonon frequency dependences observed in lead. For the temperature dependence, the misleading effects on the relaxation time are constant and can be included in the impurity relaxation-time parameter.

APPENDIX B: QUANTUM EFFECTS

Above 20 kG the surface-impedance signal gives rapid oscillations owing to quantum effects (Figs. 6 and 9). The modulated envelope of these oscillations exhibits long beats with 42.5 oscillations between beats, and their frequency $F = (18.9 \mp 0.3)$ MG corresponds to the values given in de Haas–van Alphen (dHvA) studies[9] for the smallest ζ orbit.

These observed quantum oscillations are not magnetothermal oscillations[33] but a pure surface-impedance signal, since they disappear when the microwave is off. They cannot be due to torque effects since the sample is securely fixed in the cryostat.

Quantum oscillations in surface impedance have been predicted[34] and observed in different metals,[35–37] but usually they are visible in the high-field region, above the fundametal cyclotron-resonance magnetic fields, since it is expected that cyclotron resonance is visible in the nonlocal regime $R_c > \delta$ and quantum oscillations in the local regime $R_c < \delta$.

To our knowledge, this is the first time that quantum oscillations in surface impedance have been seen in the nonlocal regime (Sec. IV C) at magnetic fields below the fundamental H_c. In addition, for a

fixed magnetic field above 20 kG, the amplitude of the dHvA signal increases with increasing the microwave frequency (Fig. 6). For the highest frequencies, in order to make the cyclotron-resonance signal visible, the amplitude of the dHvA signal can be reduced by an overmodulation obtained with a field modulation larger than the dHvA period [386 and 456 GHz in Fig. 6, and Fig. 9(a)]. In fact, at 456 GHz the dHvA amplitude is much larger than the cyclotron-resonance amplitude [Fig. 9(b)].

---

*Laboratoire associé au Centre National de la Recherche Scienfifique.

[1]S. Nakajima and M. Watabe, Prog. Theor. Phys. **29,** 341 (1963); Prog. Theor. Phys. **30,** 772 (1963).

[2]H. Scher and T. Holstein, Phys. Rev. **148,** 598 (1966).

[3]G. Grimvall, Phys. Kondens. Mater. **9,** 283 (1969).

[4]W. L. McMillan and J. M. Rowell, Phys. Rev. Lett. **14,** 108 (1965).

[5]M. Ya. Azbel' and E. A. Kaner, J. Phys. Chem. Solids **6,** 113 (1958).

[6]C. C. Grimes and A. F. Kip, Phys. Rev. **132,** 1991 (1963).

[7]W. L. McMillan and J. M. Rowell, *Superconductivity*, edited by R. D. Parks (Marcel Dekker, New York, 1969).

[8]R. T. Mina and M. S. Khaikin, Zh. Eksp. Teor. Fiz. **45,** 1304 (1963) [Sov. Phys.-JETP **18,** 896 (1964)].

[9]J. R. Anderson and A. V. Gold, Phys. Rev. A **139,** 1459 (1965).

[10]P. B. Allen, Phys. Rev. B **3,** 305 (1971).

[11]P. B. Allen and M. L. Cohen, Phys. Rev. B **1,** 1329 (1970).

[12]J. J. Sabo, Jr., Phys. Rev. B **1,** 1325 (1970).

[13]I. Krasnopolin and M. S. Khaikin, Zh. Eksp. Teor. Fiz. Pis'ma Red. **12,** 76 (1970) [JETP Lett. **12,** 54 (1970)].

[14]P. Goy, Phys. Lett. A **32,** 474 (1970).

[15]R. G. Poulsen and W. R. Datars, Solid State Commun. **8,** 1969 (1970).

[16]P. Goy and G. Weisbuch, Phys. Rev. Lett. **25,** 225 (1970).

[17]P. Goy, Doctoral dissertation (University of Paris, 1970) (unpublished).

[18]Y. Couder and P. Goy, in *Proceedings of the Symposium on Submillitimeter Waves, Polytechnic Institute of Brooklyn, Brooklyn, N. Y., 1970,* Vol. 20 of *Microwave Research Institute Symposia Series,* edited by J. Fox (Interscience, New York, 1971), p. 417.

[19]Ets. Pierre Fontaine, 20 Avenue Arago, 91-Chilly-Mazarin, France.

[20]Yu. V. Sharvin and V. F. Gantmakher, Cryogenics **5,** 278 (1965).

[21]R. G. Chambers, Proc. Phys. Soc. Lond. **86,** 305 (1965).

[22]V. P. Naberezhnykh and N. K. Dan'shin, Fiz. Tverd. Tela **12,** 2105 (1970) [Sov. Phys.-Solid State **12,** 1673 (1971)].

[23]U. Strom, H. D. Drew, and J. F. Koch, Phys. Rev. Lett. **26,** 1110 (1971).

[24]H. D. Drew, Phys. Rev. B **5,** 360 (1972).

[25]A. Kamgar, J. O. Henningsen, and J. F. Koch, Phys. Rev. B **6,** 342 (1972).

[26]The experimental evidence of resonance cutoff when the transit time given by Eq. (15) is of the order of the microwave period T, has been observed also in copper on the belly orbit ($m^* \approx 1.3 m_0$, $t \approx 1.1T$ at 457 GHz near 4 kG), and in nickel on the belly orbit [$m^* \approx 5m_0$, $t \approx T$ at 275 GHz near 15 kG; P. Goy and C. C. Grimes, Phys. Rev. B (to be published)].

[27]D. L. Dekcer, D. E. Mapother, and R. W. Shaw, Phys. Rev. **112,** 1888 (1958).

[28]R. G. Chambers, Proc. R. Soc. A **215,** 481 (1952).

[29]P. Goy and G. Weisbuch, in *Proceedings of the Twelfth Low-Temperature Physics Conference, Kyoto, 1970*, edited by E. Kanda (Keigaku, Tokyo, 1971), p. 615.

[30]P. B. Allen, in Ref. 29, p. 517.

[31]R. R. Joyce and P. L. Richards, Phys. Rev. Lett. **24,** 1007 (1970).

[32]P. Goy and G. Weisbuch, Phys. Kondens. Mater. **9,** 200 (1969).

[33]P. Goy, A. Goldstein, D. N. Langenberg, and J. C. Picard, Phys. Lett. A **25,** 324 (1967).

[34]M. Ya. Azbel', Zh. Eksp. Teor. Fiz. **34,** 1158 (1958) [Sov. Phys.-JETP **7,** 801 (1958)].

[35]E. P. Vol'skii, Zh. Eksp. Teor. Fiz. **46,** 123 (1964) [Sov. Phys.-JETP **19,** 89 (1964)].

[36]F. W. Spong and A. F. Kip, Phys. Rev. A **137,** 431 (1965).

[37]R. G. Poulsen and W. R. Datars, Phys. Rev. B **4,** 4202 (1971).